Journal of Sensor Science and Technology
Vol. 29, No. 5 (2020) pp. 283-292
http://dx.doi.org/10.46670/JSST.2020.29.5.283
pISSN 1225-5475/eISSN 2093-7563

Bluetooth Low-Energy Current Sensor Compensated Using Piecewise Linear Model

Jung-Won Shin[1+]

Abstract

Current sensors that use a Hall element and Hall IC to measure the magnetic fields generated in steel silicon core gaps do not distinguish between direct and alternating currents. Thus, they are primarily used to measure direct current (DC) in industrial equipment. Although such sensors can measure the DC when installed in expensive equipment, ascertaining problems becomes difficult if the equipment is set up in an unexposed space. The control box is only opened during scheduled maintenance or when anomalies occur. Therefore, in this paper, a method is proposed for facilitating the safety management and maintenance of equipment when necessary, instead of waiting for anomalies or scheduled maintenance. A Bluetooth 4.0 low-energy current-sensor system based on near-field communication is used, which compensates for the nonlinearity of the current-sensor output signal using a piecewise linear model. The sensor is controlled using its generic attribute profile. Sensor nodes and cell phones used to check the signals obtained from the sensor at 50-A input currents showed an accuracy of ±1%, exhibiting linearity in all communications within the range of 0 to 50 A, with a stable output voltage for each communication segment.

Keywords: Shunt current, Hall-effect sensor, Hall IC, Hall current sensor, Magneto-electric effect, Armature coil, DC voltage transducers, Bluetooth, Bluetooth-low-energy, Piecewise linear model

1. INTRODUCTION

For the past few decades, current sensors have served as parts for the over-current control of DC industrial equipment. In the future, the third industrial revolution, involving computer- and Internet-based knowledge and information, will pave the way for the fourth industrial revolution, which is centered on intelligent information technology, with keywords such as “smart” and “platform.” The transition between the third and fourth industrial revolutions has resulted in the development of smart factories. In addition to expanding and standardizing the distribution, the overall paradigm shift in industries and research and development projects related to smart factories could produce drastic changes in the future [1]. Factory-wide energy management related to production, consumption, generation, transmission, and power distribution power is required to efficiently manage, maintain, and repair various energy sources. Energy-intensive buildings and factories are currently adopting building and factory energy-management systems, respectively. In addition, home energy management systems have also been developed [2]. The structure of such smart management systems can be divided into the application program, platform, and device network, all exhibiting interoperability and security [3]. Research into smart factories is currently focused on determining the peak demand with an understanding of modeling power related to machine equipment. Simulators are also needed in areas where mechanical management and intelligent building control solutions are designed. Thus, the study can be classified into software and hardware research. However, a simulator that aids understand energy consumption modeling, determines the peak demand, and designs intelligent building control solutions using wireless sensor and actuator networks (WSAN) is required. Furthermore, in the future, current sensors will serve as software convergence devices, rather than just for blocking or controlling when an over-current over-voltage is applied. Moreover, intelligent building control solutions have been proposed for automating home applications, which minimize or control energy use by collecting and analyzing data on energy consumption, among others. These systems include intruder alarms, environment monitoring, and asset tracking setups [4-6]. Although these intelligent management systems are convenient and safe, they require expensive equipment, in addition to the installation and maintenance costs.

[1] School of Electronics Engineering, Kyungpook National Unversity IT3, Kyungpook National University, 80 Daehakro, Bukgu, Daegu 41566, Korea
[+]Corresponding author: sjw8933@daum.net
(Received: Aug. 18, 2020, Revised: Sep. 13, 2020, Accepted: Sep. 22, 2020)

Table 1. Comparison of Hall current sensor, current transformer, and shunt.

Compared items	Hall current sensor	Current transformer	Shunt
Measurement Method	Current magnetic effect	Electronic inductive	Resistance/Voltage
Measuring area	Direct current/ Alternating current over full range	Alternating current	Full range
Over current characteristics	Saturation	Destruction development	Ignition development
Linearity	0.1-0.5%	1-5%	1-5%
Required items	Power supply	Integration amplifier	Integration amplifier
Temperature characteristics	Excellent	Very good	Poor
Insulation state	Insulator	Insulator	Not insulator
Size	Small	Medium	Large

Furthermore, they are difficult to integrate with existing devices or maintenance equipment. Therefore, researchers have developed a Bluetooth current sensor that can be used with existing machinery, which facilitates the safe management of equipment. Products that utilize Bluetooth to measure the flowing current to identify and analyze the causes of malfunctions have also been developed recently and are being used in a variety of fields [7, 8]. Among the developed products that apply Bluetooth, some use the technology as a component for continuously measuring and managing the status of a device. However, when used as a mobility meter for a single device, there are cases in which the meter will be able to perform only one measurement at a time when the wire is exposed. Continuous measurements and monitoring will be difficult in such cases, and measurements will be impossible if the target is moving or vibrating. Moreover, when using current transformers capable of measuring only the AC area, in addition to the components of the current transformers being limited, measurements also become impossible in sensitive areas owing to the error rates of the output signal and software [9, 10]. Although the current Bluetooth transformer sensor described in this paper can also measure the wire current, as a measuring device, it suffers from low accuracy even with the use of Bluetooth. Rather than acting simply as a component attached to the device, the proposed Bluetooth sensor serves as a system that can perform maintenance and safety management of the device through continuous monitoring [9, 10]. The proposed Bluetooth current sensor system comprises a current sensor that uses a Hall element, a Bluetooth low energy (BLE) device for short-distance communication, and a cell-phone application for monitoring the sensor output.

2. HALL CURRENT SENSOR FOR CURRENT MEASUREMENT

Typical current sensors measure the current flowing through the wires of industrial equipment and display analog values that reflect the voltage or current measured by the current sensor mounted on a printed circuit board. The current can be measured using sensors that utilize electromagnetic induction or the current magnetic effect. As shown in Table 1, to measure the nonlinear and DC waveforms using an electromagnetic field induction, electromagnetic induction sensors add a separate circuit to measure the alternating current. When an overcurrent is produced, the measurements will be nonlinear owing to the output signal and the emergence of the destruction phenomenon [11]. Conversely, current magnetic effect sensors exhibit nondestructive properties when an overcurrent is produced. For current sensors based on the Hall effect, both direct and alternating currents can be measured using an open-loop circuit composed of silicon steel and a Hall element. Moreover, with favorable temperature characteristics, appropriate insulation of the measured current source, and excellent linearity of 0.5-1%, this sensor can be applied to products with a particular size, weight, and stability requirements.

2.1 Principle of a Current Sensor using Hall Effect

An open-loop current sensor measures the current flowing through a conductor, thus sensing the magnetic force generated in the gaps of the magnetic core. For the sensed voltage, an amplified compensation circuit is used. The generated Hall voltage can be expressed as:

$$V_H = \mathrm{K} \times \mathrm{Ic} \times \mathrm{B} \quad (1)$$

where K is a proportionality coefficient, Ic is the current applied to the Hall sensor, and B is the external magnetic flux density. When a current flows, a magnetic flux is generated in the core of the magnetic body, and a magnetic force proportional to the magnitude of the magnetic flux generates a Hall voltage in the gaps of the core. A voltage of several millivolts is generated in the Hall element, which confirms the magnitude of the magnetic

Table 2. Materials and characteristics of Hall element.

Material	Mobility (μe) (μh)	Input Current (mA)	Quiescent Hall Voltage (mV)	Input Resistance (Ω)	Output Resistance (Ω)	Product Sensitivity (mV/mA · kg)	Unbalance Voltage (mV)	Temperature Coefficient of VH (%/°C)
Ge	3600	20	≥ 5	40	30	≥ 0.25	0.5	0.02
	1800	10	≥ 5	300	200	≥ 3.0	0.5	0.02
InSb	8000	5	≥ 43	240–550	240–550	50–100	10	-1
	450	10	≥ 43	10–30	10–30	8–30	10	≤-2
GaAs	8000	5	250–550	200–800	200–800	8–20	≤ 20%	-0.05
	300		80–300					
Si	1250				(Used as Hall IC)			
	480							
InAs		400	≥30	1.4	1.1	≥ 0.075	< 1	-0.07
InAsP		100	≥14.5	5	3	≥ 0.145	< 2.0	-0.04

force. An operational amplifier can be used to amplify the output of the Hall element and measure this output as a value proportional to the current to be measured [12, 13].

2.1.1 Composition of Hall Current Sensor: Hall Element and Hall IC

Typically, a current sensor using a Hall element consists of a Hall IC, Hall element, magnetic body, and amplifying circuit. As shown in Table 2, this type of current sensor exhibits different properties depending on the characteristics of each material [12, 15]. A Hall element is a magnetic sensor that responds to magnetic fields and generally exhibits an output voltage proportional to the magnetic field. Common examples of Hall element materials include indium antimonide, indium arsenide, germanium, silicon, and gallium arsenide. A Hall IC is a combination of a compound semiconductor and a Hall element with a silicon signal-processing circuit chip [12, 14].

A Hall IC is a combination of a compound semiconductor and a Hall element with a silicon signal-processing circuit chip [12, 14]. A Hall element is an indirect-gap semiconductor as well as a wave vector semiconductor that has different electric and electronic fields. As shown in Table 2, recombination using gallium arsenide is a direct method that has greater electron mobility than that of silicon. However, gallium arsenide has the disadvantages of low heat conductivity, low intensity integration, and higher processing cost than that of normal silicon. A Hall element is made of a Gallium arsenide material but is not a high-speed analog integrated circuit [12, 14].

In this study, a Hall element with an HG-302A (AKM) sensor, which is 2.35 mm wide, 2.7 mm long, and 0.95 mm thick, was produced. The operating temperature range of the Hall sensors varies from -40 °C to 125 °C.

2.1.2 Magnetic Material

A magnetic field around a steel core occurs when a current flows through a wire crossing a magnetic core with an air gap.

Table 3 lists the magnetic materials used in current sensors [15]. Magnetic materials used in such sensors must exhibit a high permeability, high magnetic flux density, and superior saturation properties, as well as a low coercivity and low temperature

Table 3. Characteristics of magnetic materials.

Magnetic substance type & character	Silicon steel	Permalloy		Ferrite Mn-Zn	Amorphous alloy		Demand characteristics
		50Ni	80Ni		Co- based	Fe- based	
Saturation characteristics Bs (T)	2.0	1.55	0.74	0.5	0.58	1.56	> 1.0
Coercivity Hc (Oe)	0.5	0.15	0.03	0.1	0.005	0.03	< 0.1
Initial permeability	15,000	6,000	40,000	3,000	60,000	5,000	> 5,000
Top permeability	20,000	60,000	200,000	6,000	1,000,000	50,000	> 50,000
Unit resistance (μΩ/cm)	50	30	60	10	120	130	< 200
Curie characteristic Tx (°C)	750	500	500	140	255	415	> 500
Square rate Br/Bs (%)	-			30	90		> 50

dependence. However, a material with high permeability exhibits poor saturation and temperature characteristics. By contrast, materials with low permeability exhibit good saturation and temperature characteristics but poor heat-generation characteristics at high frequencies because of coercivity and iron loss. Therefore, a suitable magnetic material must be selected, based on the current measurement environment (Table 3). Silicon steel was selected as the core material for the proposed current sensor, owing to its high magnetic permeability, magnetic flux density, and saturation characteristics, as well as its low coercivity and temperature-change characteristics. Steel frames based on magnetic materials are divided into a winding coil and laminated layer according to the stratification method used. The core of the current sensor produced in this study is a directional steel core. Because the steel core is an air-gap type, the magnetic permeability is high when the magnetic field is generated in a form consistent with the direction of the steel core.

2.1.3 Amplifying Circuit

A current sensor measures the current and indicates the output of the voltage or current. To measure a magnetic field, the circuit is considered to consist of a magnetic core, a Hall element, and other electronic circuits. To express the flow of motion, an electrostatic current is supplied to operate the Hall element to measure the stimulation of the magnetic core material; subsequently, the aperture signal is output as shown in Fig. 1. In addition, the zero-offset temperature compensation of the Hall element compensates for the error characteristics according to the temperature. The phase compensation is applied by employing the compensation conditions according to the type of operational amplifier (op-amp) used, as shown in Fig. 1. In this study, an OPA2374 (Texas Instruments) op-amp was used. The expression is defined as [16]:

$$V_{out} = \frac{R2}{R1}(V2 - V1) \tag{2}$$

3. BLUETOOTH CURRENT SENSOR MANAGEMENT SYSTEM

Using an application, the Bluetooth current-sensor management system monitors the data transmitted by the wireless module using BLE through a current sensor that measures the wire current flowing through the equipment. The BLE can transmit and receive large amounts of data, with low energy consumption. The compatibility of the system with numerous mobile devices facilitates integration with multiple devices and enables multiplatform communication. This allows both a BLE with a central device connection and a peripheral device connection, as shown in Fig. 2. Fig. 2(a) shows a connection in which the BLE transfers information using an inter-device connection, to the central and peripheral devices, whereas Fig. 2(b) shows the connection status among the peripheral devices. The proposed system is composed of a Bluetooth current sensor node and a data-monitoring node, which operates using the application [17, 18].

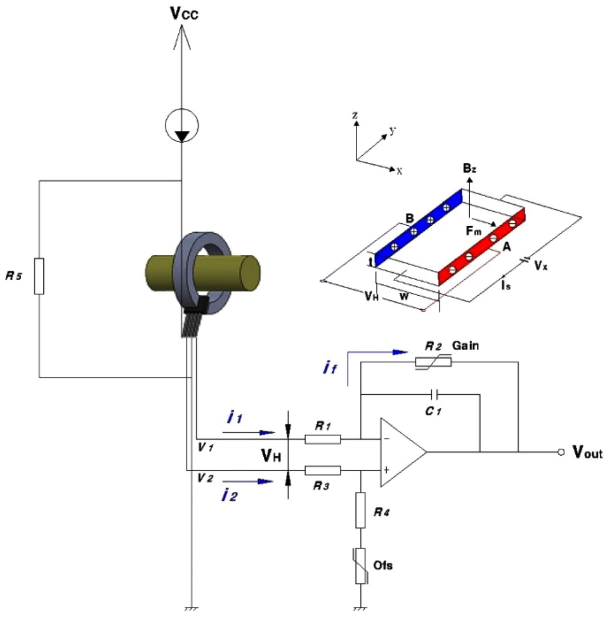

Fig. 1. Principles of open-loop current sensors with Hall element.

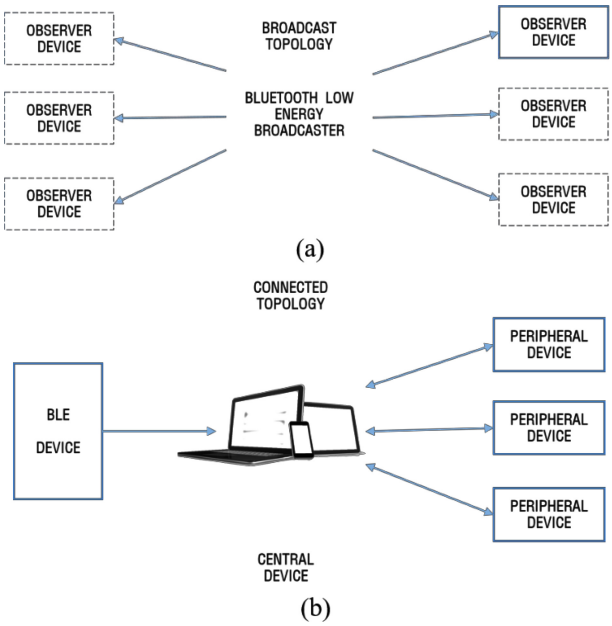

Fig. 2. Compatibility of BLE: (a) BLE broadcaster connection, (b) BLE peripheral connection.

3.1 Hardware Configuration of Bluetooth Current Sensor Node

Fig. 3(a) shows a schematic of the BLE current sensor. The BLE includes terminals that control the current sensor nodes and access the network.

Fig. 3(b) shows a flowchart of the initialization module. The hardware configuration is based on the BLE wireless protocol and Android application communication function. To display the measured analog current digitally, an ADC is used to measure the read value at the sensor node and the sensed value at a user's request, thereby initiating an ADC cycle change. An nRF52832 chip (Nordic semiconductor) that supports BLE wireless communication is used along with a 32-bit ARM Cortex M4F processor, 512 kB of flash memory, and 64 kB of SRAM. For the clock source, a 32-kHz clock can be generated internally, or a crystal can be attached externally. An external low-power 32-kHz crystal is used to increase precision. For the power supply, a DC/DC converter with low-power characteristics is used with an LC circuit in an nRF52 chip, to convert the voltage within the range of 1.7 to 3.3 V to the operating voltage of 1.3 V required by the IC [19]. A simple circuit is used for converting the analog signal (current) into a digital signal. This study also uses a successive approximation (SA) method that satisfies the requirements of both the cost and speed. Differential nonlinearity (DNL) and integral nonlinearity (INL), which are indicators of ADC nonlinearity based on a 10-bit resolution, exhibit good performance. When measuring the voltage through a SA-ADC, the converter first operates in differential mode with a 12-bit resolution to increase the signal-to-noise ratio (SNR). Subsequently, it operates in oversampling mode; the analog voltage is measured 16 times, after which the values are averaged and converted into a digital voltage. In addition, to use the temperature sensor for controlling the I2C serial communication, a two-wired interface (TWI) module, which provides a serial communication similar to that supported by the nRF52832 chip, is used. A watchdog timer is set to intervals of 30 s to reset the board in the event of temporary failures [20, 21].

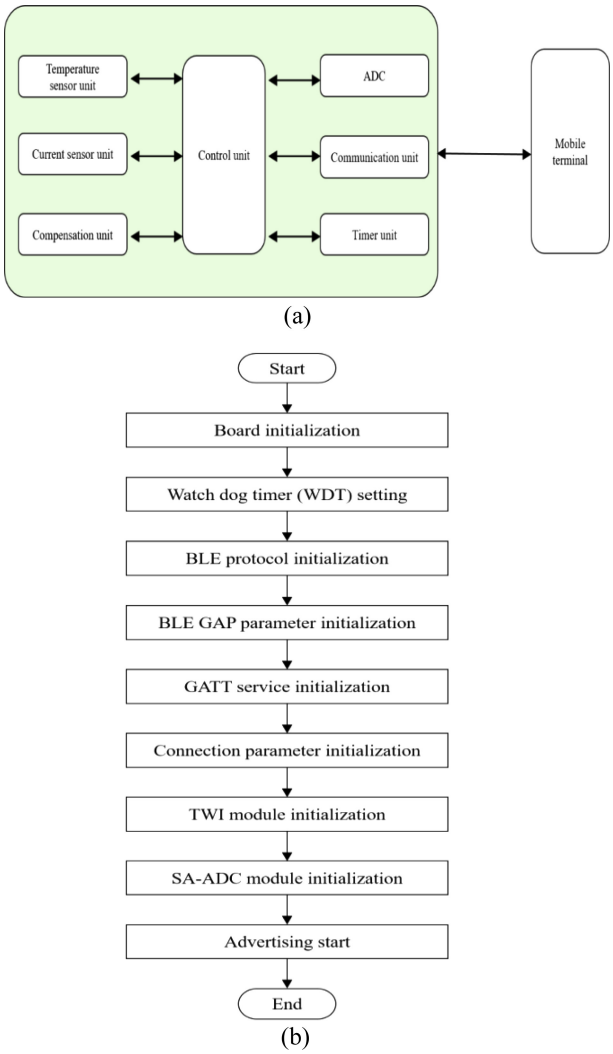

Fig. 3. (a) Configuration diagram, (b) flow chart of the BLE current sensor using module initialization method.

3.2 Software Flowchart of Bluetooth Current Sensor

The application for the proposed BLE current sensor initializes the ADC, communication unit, and timer unit of the Bluetooth sensor node (see Fig. 4).

The output voltage and ambient temperature are measured at

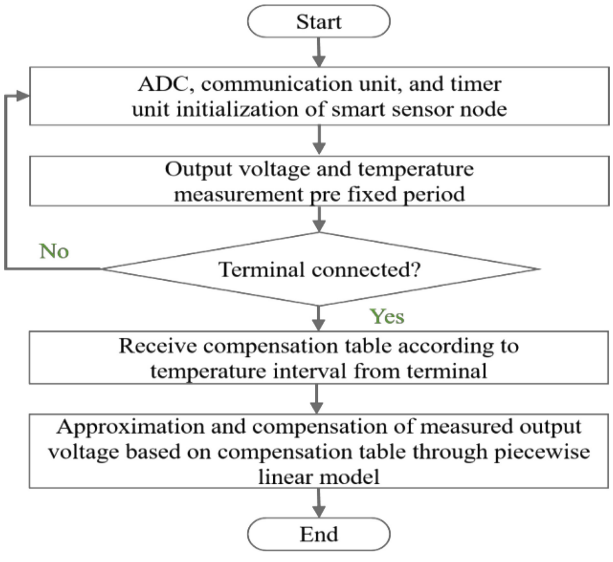

Fig. 4. Flowchart of proposed application program behavior.

regular intervals preset by the user. When the terminal is connected to the Bluetooth sensor node, the compensation table is received from the terminal, according to the temperature interval. The information to correct the voltage, rather than increase or average the measured data of the temperature interval, is obtained. Based on the current sensor output value, which depends on the temperature interval, the correction information is classified, as shown in Fig. 4, and is appropriately applied when the temperature interval changes. When the temperature interval and correction voltage information are given, the measured voltage value approximated by the piecewise linear model is corrected. If the Bluetooth sensor node and terminal are not connected, the process returns to the initialization step and repeats the measurement. When connected to the terminal, measurement is conducted by the current sensor according to the temperature measured by the temperature sensor, and the converted output voltage is approximated and compensated using the piecewise linear model. Compensating for software offset enables the system to provide a current value with a small error, and a miniaturized Bluetooth current sensor can be used without separate devices.

3.3 Empirical Compensation Equation

An empirical equation that compensates for the analog signal from the current sensor through a piecewise linear model that breaks down the voltage ranges for the measured current value can be expressed as follows:

$$\text{Compensation voltage} = B_k + \left(\frac{B_{k+1}-B_k}{A_{k+1}-A_k}\right)(V_m\text{-}A_k) \quad (3)$$

where *Vm* is the measured current sensor voltage, and *k*-values representing the information in the interval are integers between zero and 8. If the input voltage value representing the section of the measured voltage to be corrected for a specific temperature interval is assumed to be *A0–A9* (ideal case), the output voltage value of the current sensor is assumed to be *B0–B9*, and the measurement for a voltage value of lower than *A0* is between A_k and A_{k+1}, the measurement voltage is approximated according to Eq. (3). Thus, a voltage of greater than *A9* can be calculated by compensating for the voltage. The compensation information in Table 5 shows that the horizontal axis corresponds to the output voltage of the current sensor, which varies with temperature, and that the longitudinal axis corresponds to the output voltage of the ideal current sensor. When information regarding the calibration of the output voltage of the current sensor is obtained, it can be corrected in the following ways.

3.4 Reliability Verification of Proposed Bluetooth Sensor Offset

In the case of the proposed BLE current sensor, the software compensates the offset based on the compensation table given by the mobile terminal or the server to provide a smaller current with a smaller error. Thus, the offset is compensated without including any additional device to provide a smaller BLE current sensor. For the piecewise linear model, the ideal output of the current sensor is given to approximate its nonlinearity. However, as the ambient temperature is not fixed in an actual environment, correction tables (Tables 4 and 5) for calculating the output voltage interval according to the temperature can be displayed. In the corresponding graph derived from the values in the table, the horizontal axis represents the output voltage of the current sensor, which changes with temperature, and the vertical axis represents the output voltage of the ideal current sensor. Table 4 shows the output voltage value of the current sensor measured at a given temperature, and Table 5 lists the values for compensating the

Table 4. Measurement value of current sensor according to temperature section.

	Ideal	-10 °C	-5 °C	0 °C	10 °C	25 °C	40 °C	50 °C	70 °C	85 °C
Voltage	0	0.008165	0.008895	0.010015	0.012703	0.013000	0.016924	0.019028	0.230080	0.026018
	0.366	0.388	0.386	0.384	0.382	0.368	0.375	0.369	0.358	0.532
	0.733	0.768	0.766	0.761	0.753	0.745	0.731	0.721	0.696	0.676
	1.099	1.152	1.145	1.138	1.128	1.100	1.091	1.071	1.032	1.003
	1.466	1.532	1.527	1.518	1.499	1.477	1.448	1.424	1.370	1.327
	1.833	1.917	1.906	1.895	1.875	1.875	1.809	1.774	1.706	1.655
	2.199	2.298	2.289	2.275	2.247	2.212	2.166	2.127	2.044	1.979
	2.566	2.683	2.668	2.653	2.623	2.581	2.528	2.478	2.380	2.306
	2.933	3.067	3.051	3.033	2.996	2.947	2.886	2.832	2.718	2.630
	3.299	3.450	3.430	3.410	3.373	3.284	3.249	3.283	3.055	2.958

Table 5. Corrected output value according to temperature interval

	Ideal	≤ -10 °C	-10–0 °C	0–30 °C	30–50 °C	50–85 °C
Voltage	0	0.008165	0.009025	0.011906	0.017976	0.0226847
	0.366	0.388	0.386	0.378	0.372	0.4197
	0.733	0.768	0.765	0.753	0.726	0.6977
	1.099	1.152	1.145	1.122	1.081	1.0353
	1.466	1.532	1.5257	1.498	1.436	1.3737
	1.833	1.917	1.906	1.8817	1.7915	1.7117
	2.199	2.298	2.2873	2.2447	2.1465	2.050
	2.566	2.683	2.668	2.619	2.503	2.388
	2.933	3.067	3.0503	2.992	2.859	2.7267
	3.299	3.450	3.430	3.3557	3.266	3.0987

output voltage value of the current sensor according to the temperature interval. The compensation of the current values measured by the current sensors can be applied using a partially linear model by dividing the voltage intervals for a given measured current. To approximate the nonlinear characteristics of the current sensor with a partially linear model, information regarding the ideal output value of the current sensor and the actual output value is required according to the temperature. As shown in Table 4, the average value of the specific current sensor output voltage is calculated at −10 °C, −5 °C, 0 °C, and 10 °C. Table 5 shows the compensation information for sections 50 °C – 85 °C and at 0 °C to 30 °C. Voltage correction information can be obtained in a direction that reduces errors. Once the calibration information of the current sensor output voltage for the temperature interval is obtained, a compensation experiment (3) can be conducted to calibrate the specific voltage value approximated using the partial linear model (see Fig. 5).

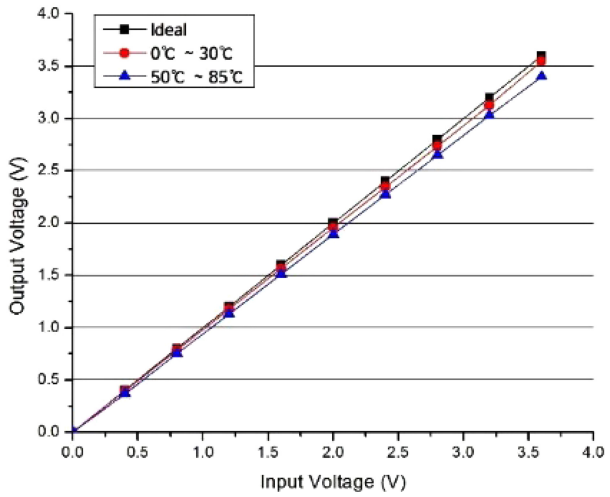

Fig. 5. Compensation graph.

3.5 Fabrication of Proposed Smart Current Sensor

The proposed smart current sensor was designed to digitize the analog output of the current sensor and transmit data to the application via Bluetooth communication. Fig. 6 shows the proposed smart current sensor circuit. The proposed BLE current sensor can be divided into the current sensor unit and the Bluetooth unit.

Fig. 6(a) shows the proposed smart current sensor. The dimensions of the silicon steel core are as follows: inner diameter of 8 mm, an outer diameter of 12 mm, a thickness of 10 mm, and an air gap of 1.5 mm. As shown in Fig. 1, the Hall element is inserted between the pores of the silicon steel, and when the

(a)

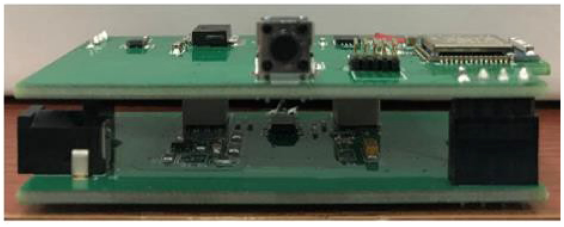

(b)

Fig. 6. (a) Proposed BLE current sensor, (b) laminated BLE current sensor module.

magnetic field is applied to the Hall element, the Hall voltage is amplified relative to the magnitude of the magnetic field, as shown in Eq. (2). Fig. 6(b) shows the DC/DC converter used to control the difference between voltages [11]. The characteristic frequency of the current sensor is 25 kHz. The linearity of the output relative to the rated current is 1%. The circuit of the BLE current sensor is stacked to achieve a ground design that does not cause errors owing to interference between the current sensor, controller, and Bluetooth device. This also minimizes the footprint of the circuit.

Fig. 7 shows the configuration of the Android app used in the completed Bluetooth current sensor experiment. When the monitoring app is launched on a phone screen, it scans the area for 10 s to detect nearby BLE devices. After finding the available BLE devices, the user selects the device to be connected. A connection with the BLE device is established and information is then exchanged between the app and BLE device. The connection status, temperature received from the smart sensor node, data communication cycle, current sensor model number, and measured current can be monitored through the smartphone app. The measured current value can be saved as a text file (Fig. 7(b)). The data are stored from the time the user presses the "Start" button until when the user presses "Stop" on the application screen.

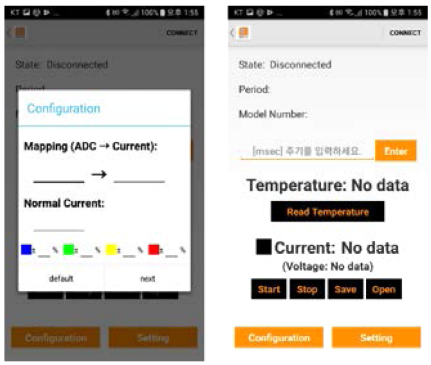

(a) (b)

Fig. 7. Proposed BLE current sensor application: (a) configuration, (b) data channels.

4. EXPERIMENT AND RESULTS

4.1 Measurements and Tests

Experiments were conducted based on the theoretical backgrounds of the current sensor and the currently used methods. A voltage of ±15 V was supplied to drive the current sensor; in addition, DC (KIKUSUI PWR1600L) and AC (KAST S2307180) devices were used to provide the wire current flows for the measurements, and a stable current was therefore supplied. To inspect the linearity of the Bluetooth current sensor for a 4 V output at a rating of 50 A, we increased the current in steps of 5 A; compared the information displayed in the BLE sensor, PCB output stage, and screen of the cell-phone application; and, evaluated the measurement accuracy. Here, two multimode (KEYSIGHT 34461A) measuring devices were connected to measure the output signals of the BLE sensor and PCB separately. The direct and alternating currents were measured using different power sources, and the linearity and accuracy of the output values were plotted as shown in Fig. 8 [12]. In addition, an experiment was conducted to compensate for the temperature of the current sensor for other input currents, and the results were tested using an anti-temperature humidifier (JEIOTECH HG-G-1000) for 10 s, by varying the input current and reaching a temperature of −10 °C to 85 °C.

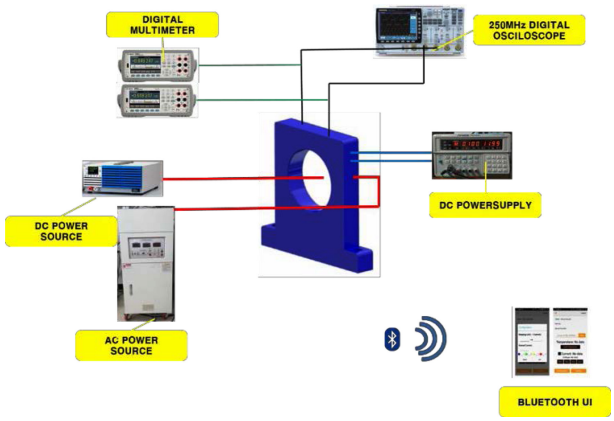

Fig. 8. Schematic of proposed BLE current sensor experiment.

4.2 Experimental Results of the Proposed Bluetooth Sensor

After installing the proposed sensor in various environments, to evaluate the accuracy of the measured output displayed on the smartphone, we compared the outputs of the proposed sensor and the power supply. We evaluated the accuracies of the same measurements in both the sensor PCB and application. We also compared the output value for the input current with direct and alternating currents (see Fig. 9(a) and (b)). Simultaneously, to measure the ideal output values for the input current and output voltage of the sensor, PCB, and application, and to evaluate the accuracy of the measurements for each input voltage, we

increased the input voltage in 5 A increments from 0 to 50 A, and compared the voltage measured at each part by the sensor, PCB, and application. To measure and monitor the output voltage values in the DC and AC areas, the output for each input value was measured at three positions using the smartphone app screen and two digital multimeters. Fig. 9 shows the linearity and accuracy of the measured values of the current sensor.

The entire area showed linearity within 1%, and the current sensor, PCB, and app exhibited stable values within 0.05% for the input current when comparing the error rates for the DC and AC measurements. At 45 A, the value measured by the sensor showed the highest rate of change, with an output voltage of 0.1 V. Compared to the rest of the area, this value was also stable within 1%. To evaluate the Bluetooth sensor for comparison, this study measured the current flowing through the wire under the same load conditions. The current input into the Bluetooth sensor, the current flowing through the PCB, and the value measured by the Bluetooth sensor and displayed on the tablet computer all showed stable output values with an error of within 1%.

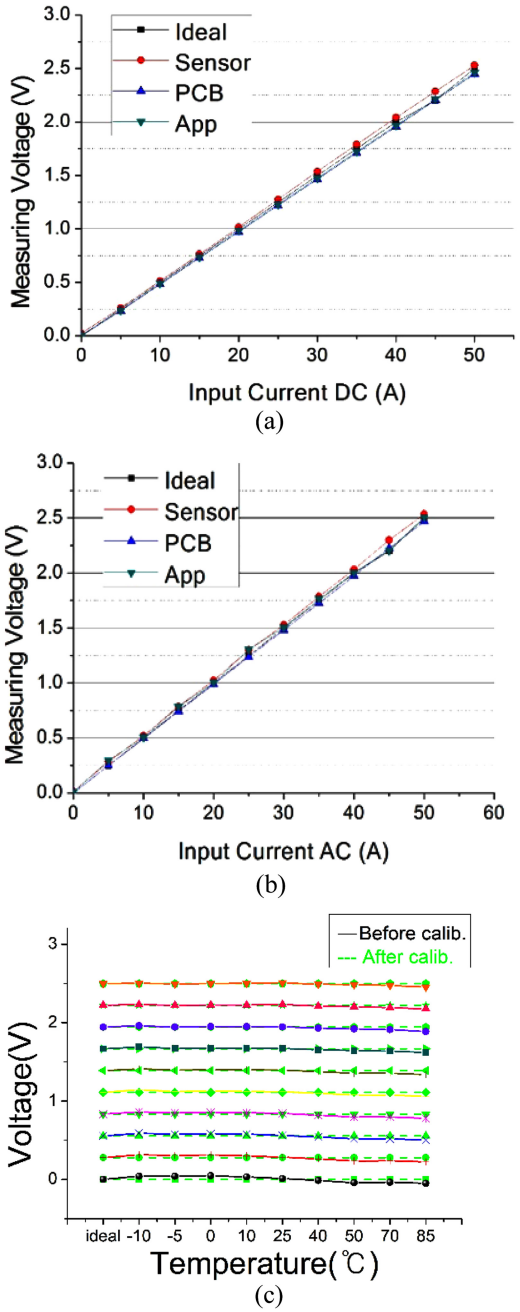

Fig. 9. Comparison of measurement data from different parts with input current: (a) Comparison of direct current measurements, (b) comparison of alternating current measurements, (c) a comparison graph.

Fig. 9(c) shows the ideal output value for the values obtained experimentally, with an output voltage of 100 A to 2.5 V at different rated currents, while varying the temperature between −10 °C and 85 °C. The value of the overall measurement error is shown in the graph; the higher the output reference temperature interval, the greater the rate of change in the corrected width of the compensation value than that in the other temperature segments.

5. CONCLUSIONS

In this study, the installation of a BLE-based current sensor system in a location unexposed to the surrounding environment was proposed. Unlike previously developed portable current measurement devices, the proposed system utilizes software to compensate for the offset andnonlinearity of the Bluetooth current sensor, without any additional equipment. After measuring the current in the current sensor, the output voltage could be obtained, transmitted, recorded, monitored in real-time, displayed, and stored. The main characteristic of the proposed BLE current sensor is its use of BLE technology, which reduces power consumption. It can also be used in the mounting spaces of existing current sensors, thus eliminating problems with mobility and flexibility between systems. By consistently stabilizing, maintaining, and managing the equipment via continuous monitoring, its efficiency and lifetime can be increased. Moreover, the linearity of the output values sensed without distinguishing between the DC and AC areas exhibited excellent accuracy, with an error of less than or equal to 1%. In addition, when other rated values of the same circuit were measured, accuracy and linearity of less than 1% were observed.

Depending on the area where the current sensor is to be mounted and measured, the material of the component attached to the current sensor will vary. In the case of silicon steel, which is the material used for the cores, the sensitivity within the low

current range is improved, whereas the coverage area is low because of the low saturation. In the future, we plan to conduct a primary study on this part to show that it results in better-performing current sensors through hysterical curves and a magnetic field analysis using the core characteristics. When the rated value of a circuit other than the same circuit is measured, the data are verified by receiving the compensation table according to the temperature interval and using the output value of the ideal table to compensate the measured output voltage approximating the partially linear model. For devices other than current sensors, future studies should focus on whether the software can be implemented for offset compensation.

ACKNOWLEDGMENT

The authors would like to thank Hankook Sensor Co., Ltd., South Korea, for the technical and technological support provided during system development and characterization. This work was supported in part by the Daegu Technopark Nano Convergence Practical Application Center of South Korea.

REFERENCES

[1] E. K. Jeon, "Legislation and policy issues", https://www.sensors.or.kr/ (retrieved on Sep. 8, 2012).
[2] M. Farrokhifar, F. Momayyezi, N. Sadoogi, and A. Safari, "Real-time based approach for intelligent building energy management using dynamic price policies", *Sustain. Cities Soc.*, Vol. 37, pp. 85-92, 2018.
[3] F. Clarizia, D. Gallo, C. Landi, M. Luiso, and R. Rinaldi, "Smart meter systems for smart grid management", *Proc. 2016 IEEE Internat. Instrum. Meas. Technol. Conf.*, pp. 1-6, Taipei, Taiwan, 2016.
[4] M. P. Fanti, A. M Mangini, and M. Roccotelli, "A simulation and control model for building energy management", *Control Eng. Pract*., Vol. 72, pp. 192-205, 2018.
[5] E. D. Lipson and B. D. Horwitz, *"Photosensory reception and transduction" in Sensory Receptors and Signal Transduction*, J. L. Spudich and B. H. Satir, Eds. Wiley-Liss, New York, pp. 1-64, 2001.
[6] J. S. Han, C. S. Choi, W. K. Park, I. W. Lee, and S. H. Kim, "Smart home energy management system including renewable energy based on ZigBee and PLC", *IEEE Trans. Consum. Electron.*, Vol. 60, No. 2, pp. 198-202, 2014.
[7] S. Abdelmalek, L. Barazane, A. Larabi, and M. Bettayeb, "A novel scheme for current sensor faults diagnosis in the stator of a DFIG described by a TS fuzzy model", *Measurement*, Vol. 91, pp. 680-691, 2016.
[8] C. Gan, J. Wu, Y. Hu, S. Yang, W. Cao, and J. L. Kirtley, "Online sensorless position estimation for switched reluctance motors using one current sensor", *IEEE Trans. Power Electron*., Vol. 31, No. 10, pp. 7248-7263, 2016.
[9] S. C. Yang, "Saliency-based position estimation of permanent magnet synchronous machines using square-wave voltage injection with a single current sensor", *IEEE Trans. Ind. Appl*., Vol. 51, No. 2, pp. 1561-1571, 2015.
[10] C. Chakraborty and V. Verma, "Speed and current sensor fault detection and isolation technique for induction motor drive using axes transformation", *IEEE Trans. Ind. Electron*., Vol. 62, No. 3, pp. 1943-1954, 2015.
[11] H. Yan, Y. Xu, W. Zhao, H. Zhang, and C. Gerada, "DC drift error mitigation method for three-phase current reconstruction with single Hall current sensor", *IEEE Trans. Magn.*, Vol. 55, No. 2, pp. 8100604(1)-8100604(4), 2019.
[12] J. W. Shin, B. S. Choi, and Y. H. Ha, *J. Sci. Technol.,* Vol. 24, No. 3, pp. 194-201, 2015.
[13] N. Castro, S. Reis, M.P. Silva, V. Correia, S. Lanceros-Mendez, and P. Martins, "Development of a contactless DC current sensor with high linearity and sensitivity based on the magnetoelectric effect", *Smart Mater. Struct*. Vol. 27, No. 6, pp. 065012(1)-065012(6), 2018.
[14] J. S. Kim, "Study of closed loop electric current sensors of 3 core-4 winding mode", M. S. thesis, Kumoh National Institute of Technology, Gumi-Si, South Korea, 2008.
[15] A. Itzke, R. Weiss, and R. Weigel, "Influence of the conductor position on a circular array of Hall sensors for current measurement", *IEEE Trans. Ind. Electron*., Vol. 66, No. 1, pp. 580-585, 2019.
[16] J. H. Park, "Study of automotive current sensor using hall effect of open loop type", M. S. thesis, Incheon University, Incheon, South Korea, 2013.
[17] M. Rewienski and J. White, "A trajectory piecewise-linear approach to model order reduction and fast simulation of nonlinear circuits and micromachined devices", *IEEE Trans. Comput. Aided Des. Integr. Circuit Syst.,* Vol. 22, No. 2, pp. 155-170, 2003.
[18] https://www.tta.or.kr/data/web.jsp (retrieved on Jul. 24, 2001).
[19] http://www.nordicsemi.com (retrieved on Dec. 2015).
[20] B. Yu, L. Xu, and Y. Li, "Bluetooth Low Energy (BLE) based mobile electrocardiogram monitoring system", *IEEE Int. Conf. Inf. Autom*., pp. 763-767, Shenyang, China, 2012.
[21] P. Kriz, F. Maly, and T. Kozel, "Improving indoor localization using Bluetooth low energy beacons", *Mob. Inf. Syst*., Vol. 2016, pp. 2083094(1)-2083094(11), 2016.